Content available at Bio-Research

Journal of Biological Research and Biotechnology
Journal Home page: https://bio-research.com.ng/index.php/home

ORIGINAL ARTICLE

Synthesis and Preliminary Physicochemical Characterization of Medicinal Plant Extract-Loaded Hyaluronic Acid–Chitosan Nanoparticles for Cancer Drug Delivery

[1*]Joy I. Odimegwu, [2]Irene S. M. Rodríguez, [2]Viviana J. G. Velázquez, and [2]Ester V. Fernández-Pacheco.
[1]Department of Pharmacognosy, Faculty of Pharmacy, University of Lagos, Nigeria.
[2]MSOC NanoChemistry group, Departamento de Química Orgánica, Facultad de Ciencias y Tecnologías Químicas-IRICA, University of Castilla-La Mancha, 13071 Ciudad Real, Spain.

ARTICLE INFO

Received: 25th July 2026
Revised: 22nd August 2026
Accepted: 24th August 2026
Published online: 31st August 2026
DOI: https://dx.doi.org/10.4314br.v24i2.4

Publisher's Note: *Bio-Research remains neutral with regard to jurisdictional claims in published maps and institutional affiliations. Bio-Research or its licensor (e.g. a society or other partner) holds exclusive rights to this article under a publishing agreement with the author(s) or other rightsholder(s); author self-archiving of the accepted manuscript version of this article is solely governed by the terms of such publishing agreement and applicable law.*

e-ISSN: 2705-3822
print-ISSN: 1596-7409

Official. Faculty of Biological Sciences, University of Nigeria.

ABSTRACT

Cancer therapy is continually hindered by poor drug bioavailability, off-target systemic toxicity, and evolving multidrug resistance. This study developed and characterized polymeric nanoparticles (PNPs) for targeted delivery of apoptotic phytochemicals from Annona muricata leaves (AmE), Bryophyllum pinnatum leaves (BpE), and Dioscorea rotundata tubers (DrE), formulated separately. A smart delivery vehicle was synthesised using hyaluronic acid and chitosan, selected for their biocompatibility and mucoadhesive properties. The PNPs were prepared by polyelectrolyte complexation. Dynamic light scattering (DLS) evaluated nanoparticle configuration, UV–Vis spectroscopy provided qualitative evidence of extract incorporation, and FTIR identified functional groups responsible for polymer–extract conjugation. Surface and internal structures were visualised using scanning electron microscopy and transmission electron microscopy. DLS showed mean hydrodynamic sizes of 535.6 nm, 450.5 nm, and 344.8 nm for AmE, BpE, and DrE PNPs, respectively, with corresponding polydispersity indices of 0.264, 0.292, and 0.254. All three formulations demonstrated preliminary successful encapsulation within stable polymeric matrices, supported by optical evidence from UV–Vis and chemical evidence from FTIR. DrE produced the smallest and most uniform particles. Morphological analysis revealed optimised spherical particle distributions, which are critical for cellular uptake and sustained release. Formulating AmE, BpE, and DrE in efficient polysaccharide nanocarriers establishes a robust framework for precise, smart drug delivery. These plant-derived PNPs offer a promising biocompatible alternative to conventional chemotherapy delivery, potentially enhancing efficacy while minimising systemic adverse effects. Studies are ongoing to attain desirable particle sizes and distributions for subsequent drug-delivery experiments. Further optimization will support the intended application of these formulations in targeted anticancer therapy.

Keywords: *Bryophyllum pinnatum*; Herbal medicine; Hyaluronic acid; Nanoparticles; Drug delivery; Polyelectrolyte complexation.

Cite this article: Odimegwu, J. I., Irene, S. M. R., Viviana, J.G. V., & Ester, V. F. P. (2026). Synthesis and preliminary physicochemical characterization of medicinal plant extract-loaded hyaluronic acid–chitosan nanoparticles for cancer drug delivery. Journal of Biological Research and Biotechnology. 24(2), 540-549.
Corresponding author: Odimegwu[1] J. Ifunanya. Email: jodimegwu@unilag.edu.ng. DOI: https://dx.doi.org/10.4314br.v24i2.4

1.0 INTRODUCTION

Cancer is a major cause of premature death globally. In sub-Saharan Africa, cancer represents an escalating global health crisis, with its disease burden falling disproportionately on low- and middle-income regions. In sub-Saharan Africa, late-stage presentation, driven by constrained infrastructure for early detection and limited access to advanced therapeutic interventions, results in significantly elevated mortality-to-incidence ratios compared to global averages (WHO, 2024). The disease burden is quite severe in low- and middle-income countries. Conventional treatments such as chemotherapy and radiotherapy are often effective; however, they are also associated with systemic toxicity, poor selectivity, and the development of multidrug resistance (Siegel et al., 2023). The listed limitations have led to the search for more precise, biocompatible, and sustainable therapeutic strategies, in which nanotechnology has emerged as a welcome transformative approach. Nanotechnology, using natural products, promotes sustainability, biocompatibility, and minimal negative ecological impact (Edo et al., 2025). In cancer therapy, this approach leads to the creation of smart drug delivery systems that enhance therapeutic efficacy while reducing harm to healthy tissues. The reported study explores the development and characterisation of HA-CS-based polymeric nanoparticles loaded with bioactive plant extracts from *Annona muricata* (Soursop leaves), AmE, *Bryophyllum pinnatum* (Life plant) BpE, and *Dioscorea rotundata* (White yam tubers) DrE. These plants, widely used in African traditional medicines, are rich in phytochemicals with documented anticancer properties. AmE contains acetogenins, Annomuricin A, B, and C, known to induce apoptosis and inhibit mitochondrial complex I in cancer cells (Moghadamtousi et al., 2015 & Yu et al., 2023, Ubhenin, 2026). BpE is a source of bufadienolides, namely Bryophyllin A, B, C, and Bersaldegenin-3-acetate, which modulate autophagy and reverse drug resistance (Ojewole, 2005). DrE a staple in most of Africa, offering steroidal saponins and diosgenin—compounds that interfere with cell proliferation and angiogenesis (Odimegwu **et al**., 2022 and Nwogha **et al**., 2023).

The rationale for using whole plant extracts rather than isolated compounds lies in the potential for synergistic interactions among phytochemicals, which possibly enhance therapeutic outcomes and reduce the likelihood of drug resistance, which is already rampant (Wagner, 2011). However, the clinical translation of these plant extracts is hindered by poor solubility, instability, and non-specific distribution. Encapsulating them within HA-CS nanoparticles addresses these challenges by improving pharmacokinetics, protecting the compounds from degradation, and enabling targeted delivery to tumor sites. Crucial to this innovation is the use of polymeric nanoparticles (PNPs), which are nanoscale carriers engineered to encapsulate and deliver therapeutic agents at cancer sites with high precision. PNPs have many advantages over conventional drug delivery systems, including advanced and efficient controlled release, improved solubility of hydrophobic drugs, and the ability to bypass biological barriers (Misra et al.,, 2022). Hyaluronic acid (HA) and chitosan (CS) are natural polymers, and their nanoparticles show excellent biocompatibility (Merino et al., 2015), biodegradability, and inherent

Copyright @2026 – Journal of Biological Research and Biotechnology . All Rights Reserved. | By Afrischolar Discovery

targeting capabilities. HA binds selectively to CD44 receptors overexpressed on many cancer cells, while CS enhances mucoadhesion and cellular uptake (Dash et al., 2021; Rinaudo, 2006, Onuigbo et al., 2020). Moreover, the use of HA and CS as base polymers reflects a commitment to biological safety. HA is a naturally occurring glycosaminoglycan found in connective tissues, while CS is derived from chitin, a waste product of the seafood industry (Rinaudo, 2006). Their use not only reduces reliance on synthetic polymers but also promotes circular bioeconomy principles. The combination of these polymers creates a versatile matrix capable of encapsulating diverse phytochemicals and adapting to various therapeutic needs. The formulation process used ionic gelation and nano-precipitation techniques, which are compatible with green chemistry principles. The characterization methodology included particle size analysis, encapsulation efficiency, and morphological assessment using scanning electron microscopy (SEM) and transmission electron microscopy (TEM). Spectroscopic techniques such as Fourier-transform infrared spectroscopy (FTIR) and ultraviolet-visible (UV-Vis) spectroscopy are typically employed to confirm successful loading and interaction between the polymers and plant extracts (Mukherjee **et al**., 2023). The ultimate goal is to demonstrate that PNPs can be loaded with bioactive plant extracts successfully and in the future, be used to selectively deliver therapeutic agents to cancer cells, minimizing off-target effects and maintaining sustained drug release. This research aligns with global efforts to effectively modify cancer treatment by leveraging locally available medicinal plants and low-cost nanocarriers. In resource-limited settings such as Nigeria, where access to advanced therapeutics is constrained, nanotechnology offers a viable pathway to develop affordable and effective cancer therapies. Mechanistically, the PNPs are usually designed to exploit the enhanced permeability and retention (EPR) effect for drug loads. This passive targeting is further enhanced by the active targeting capabilities of HA, which binds to CD44 receptors, facilitating internalization into cancer cells. Once inside the diseased cell, the acidic microenvironment triggers the release of the encapsulated bioactive extracts, initiating apoptosis and disrupting cellular metabolism (Maeda, 2015).

The novelty of this study lies in its multifaceted approach, combining synthesis, polymeric engineering, ethno-botanical knowledge, and cancer biology to create a next-generation drug delivery system. The work goes beyond proof of concept by studying a scalable, reproducible, and clinically relevant formulation strategy. The integration of three distinct plant extracts allows for comparative analysis of efficacy and stability, providing valuable insights into the design of personalised nanomedicines. Conclusively, the primary aim of this research is to synthesize and characterize a novel biopolymeric delivery platform by leveraging the electrostatic complexation between hyaluronic acid and chitosan, which is designed to effectively encapsulate chemically diverse bioactive extracts from AmE, BpE, and DrE,

2. MATERIALS AND METHODS

2.1. Plant collection and identification

The plants were authenticated at the University of Lagos Herbarium and assigned the following numbers: *Annona muricata is* LUH 9758. *Bryophyllum pinnatum* is LUH 6882, and *Dioscorea rotundata* is TDr/1669 from the International Institute of Tropical Agriculture (IITA), Ibadan, Nigeria.

2.2 Plant extract preparation

Authenticated plant parts (*Annona muricata* leaves, *Bryophyllum pinnatum* whole plant, and *Dioscorea rotundata* (tubers) were thoroughly washed with distilled water, shade-dried for 2 weeks at ambient room temperature (25 ± 2°C), and pulverised into fine powders using a commercial mechanical grinder. For extraction, 100 g of ground powder of *A. muricata* and *B. pinnatum* were independently macerated in 1 liter of 96% aqueous ethanol, while *D. rotundata* powder; 100 g was macerated in 1 liter of 70% aqueous ethanol under constant agitation for 72 h at room temperature. The mixtures were filtered through clean cotton cloth.

The filtrates were dried by evaporation at room temperature . Concentrates were stored at 4°C in airtight glass vials prior to nano-encapsulation.

2.3 GC-MS Characterisation

GC-MS analysis was carried out following the Chromatographic conditions described by Gavamukulya et al. (2015) for AmE, Okafor et al. (2024) for BpE and Nwogha et al. (2023) for DrE.

2.4. Preparation of HA-CS nanoparticles

Hyaluronic acid–chitosan nanoparticles (PNPs) were prepared via polyelectrolyte complexation based on the amended Liu **et al**. (2015) approach:

Chitosan solution: 10 mg of CS was dissolved in 10 mL of 2% acetic acid. Hyaluronic acid solution: 10 mg of HA was dissolved in 10 mL of Milli-Q water.

Complexation mechanics: The HA solution was added drop-wise to the CS solution under constant stirring at 200 rpm for 1 h until an opalescent solution formed.

Purification: The resulting mixture underwent dialysis using a membrane with a molecular weight cut-off (MWCO) of 6–8 kDa for 6 to 24 hours to effectively remove unreacted residues.

2.5. Drug loading procedure

Plant extracts, AmE, BpE and DrE were loaded separately into the blank nanoparticles by mixing 1 mL of the extract solution (concentration: 1 mg/mL) with every 8 mL of the blank nanoparticle suspension. The final formulation was filtered using a 0.45 µm nylon pore filter to ensure uniformity in size.

Loading capacity (LC%)

Mass of encapsulated extract / mass of extract-loaded nanoparticles × 100

2.6. Characterisation of nanoparticles

The synthesized nanocarriers were characterized using the following analytical methods: Physicochemical Analysis: Ultraviolet-visible (UV-Vis) spectroscopy. UV–visible spectra of the free extracts, extract-loaded nanoparticles and unloaded HA–CS nanoparticles were recorded over 200–800 nm. Unloaded HA–CS nanoparticles served as the formulation control. The spectrophotometer was zeroed using Milli-Q water. While Fourier-Transform Infrared Spectroscopy (FTIR), the spectra of the unloaded and extract-loaded HA–CS nanoparticles were recorded over 4000–600 cm^{-1} at a resolution of 4 cm^{-1} using direct measurement. Each spectrum represented 3 scans and was used to identify functional groups.

Size Distribution: Dynamic Light Scattering (DLS) The hydrodynamic diameter and polydispersity index were measured by dynamic light scattering using a 90Plus particle-size analyzer (Brookhaven Instruments Corporation, Holtsville, NY, USA), equipped with a 640 nm diode laser and operating at a scattering angle of 90°. Measurements were performed at 25°C for 6 min, with three independent measurements conducted for each formulation to monitor particle size throughout various preparation stages, including post-dialysis and dilution with distilled water.

Morphological Analysis: Scanning Electron Microscopy (SEM) and Transmission Electron Microscopy (TEM) were utilized to observe the physical configuration and vesicle structure of the particles.

2.7 Sample preparation for microscopy

Samples were prepared both with and without lyophilisation. SEM samples were applied to grids or dropped/attached to pins to optimize imaging time. The following method was used: nanoparticle suspension was deposited onto formvar-coated copper grids and allowed to dry at room temperature. Samples were unstained. SEM imaging was conducted using a ZEISS GeminiSEM 500 field-emission microscope at an accelerating voltage of 2.0 kV, an approximately 3.3 mm working distance, and an InLens secondary-electron detector. TEM images were acquired using a JEOL JEM-1400 transmission electron microscope (JEOL Ltd., Tokyo, Japan) operated at 120 kV.

3.0 RESULTS

3.1. Phytochemical profiling of bioactive extracts

GC–MS analysis revealed distinct chemical profiles among the three plant extracts (Tables 1 to 4). The ethanolic leaf extract of AmE; Table 1 contained fatty acids, fatty alcohols, aldehydes, esters, and terpenoid-related compounds. The major identified constituents were (Z)-tetradec-7-enal (9.39%), hexadecanoic acid, also known as palmitic acid (7.12%), etc. The polar extract of BpE; Table 2 was dominated by 3-eicosene (E)

(16.40%); tritetracontane (15.64%), etc. were detected. The nonpolar BpE extract in Table 3 contained methyl 11-octadecenoate (19.28%), Z,Z-6,13-octadecadien-1-ol acetate (17.21%), 12-methyl-E,E-2,13-octadecadien-1-ol (10.26%), oleic acid (10.22%), etc. as its principal constituents. These results indicate that the BpE fractions were predominantly composed of long-chain hydrocarbons, unsaturated fatty acids, fatty-acid esters, aldehydes, and alcohol derivatives. DrE; Table 4 comprised metabolites distributed among fatty acids, lipids, sugars, amino acids, nucleotides, alcohols, esters, coumarins and other chemical groups.

3.2. **Physicochemical characterisation of HA-CS nanoparticles**

Dynamic Light Scattering (DLS) confirmed the successful synthesis of polyelectrolyte complex nanoparticles (PNPs) (Figures 1-3). The transition from clear individual solutions of Hyaluronic Acid (HA) and Chitosan (CS) to an opalescent suspension indicated the formation of stable nanostructures. Comparative DLS measurements across various preparation stages, including post-dialysis and dilution, monitored the colloidal stability and size distribution of the particles. FTIR spectroscopy (Figure 7) provided evidence of the chemical interactions between the polymers and the loaded extracts. Characteristic peaks were observed at 3300 cm^{-1} (O-H stretching), 2900 cm^{-1} (C-H stretching), and 1700 cm^{-1} (C=O stretching). The spectral fingerprint in the 1200-1000 cm^{-1} region (C-O stretching) further supported the presence of alcohols and carboxylic acids inherent to the plant extracts within the HA-CS matrix.

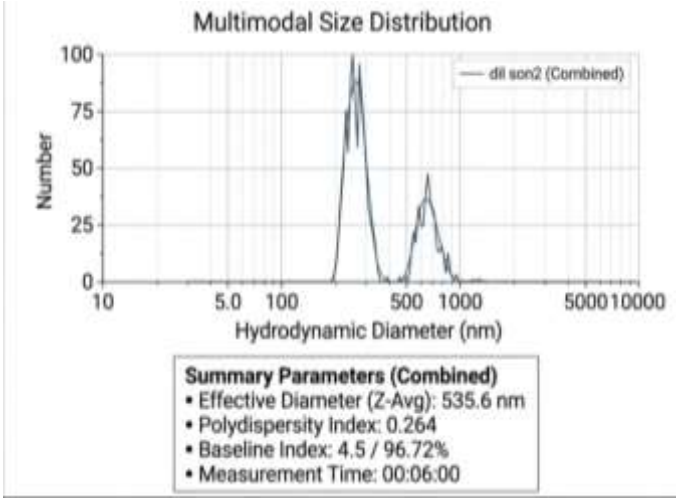


Figure **1.** Particle size characterization of AmE. Hydrodynamic size distribution measured by Dynamic Light Scattering (DLS) showing a mean Z-average diameter of 535.6 nm ± 6.0 nm. The polydispersity index (PDI) of 0.264 indicates a stable, moderately uniform distribution. Data represent the mean of three independent measurements (n = 3).

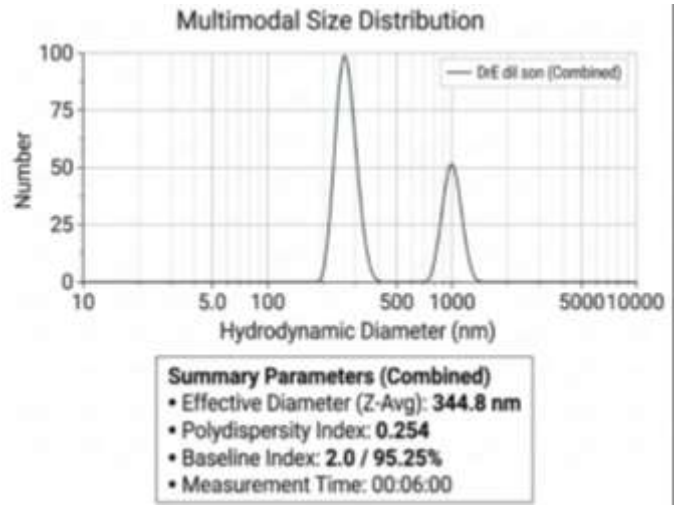


Figure **2.** Particle size characterisation of BpE. Hydrodynamic size distribution measured by Dynamic Light Scattering (DLS) showed a mean Z-average diameter of 450.5 nm ±6.0 nm. The polydispersity index (PDI) of 0.264 indicates a stable, moderately uniform distribution. Data represent the mean of three independent measurements (n = 3).

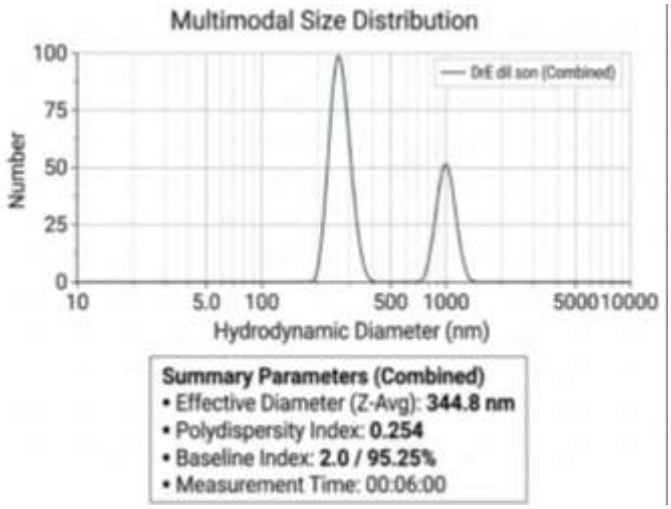


Figure 3 Particle size characterisation of DrE. Hydrodynamic size distribution measured by Dynamic Light Scattering (DLS) showed a mean Z-average diameter of 344.8 ± 6.0 nm. The polydispersity index (PDI) of 0.254 indicates a stable, moderately uniform distribution. Data represent the mean of three independent measurements (n = 3).

3.3. UV-Vis spectroscopic confirmation of loading

UV-Vis spectrophotometry (Figures 4, 5, and 6) was employed to assay the loading of the crude drug extracts. The characterization experiments confirmed that the crude extracts were efficiently loaded into the (PNP) system.

Chitosan: 10 mg in 10 mL, Hyaluronic acid: 10 mg in 10 mL, 8 mL × 20 mg = 8 mg polymer.

Each formulation received 1 mL × 1 mg/mL = 1 mg extract.

$$LC\ (\%) = (1/8 + 1) \times 100 = 11.1\% \quad (1)$$

Based on the formulation inputs, the maximum theoretical extract-loading capacity was 11.1% w/w.

Therefore, as a percentage of the total loaded nanoparticles, it is 12.5% w/w:

$1/8 \times 100 = 12.5\%$

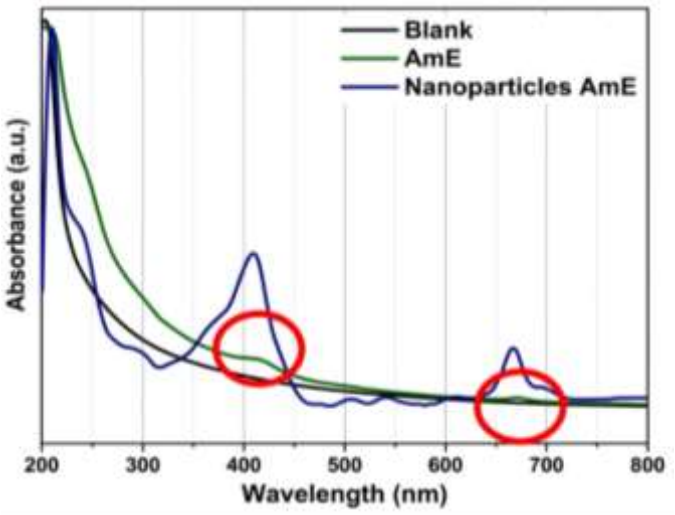


Figure **4**. UV-Vis characterization of AmE-loaded polymeric nanoparticles. UV-Vis absorption spectra of pure AmE extract (green line), blank HA-CS nanoparticles (black line), and AmE-loaded HA-CS nanoparticles (blue line). The two red analytical circles, one highlighting the subtle shoulder in the BpE curve at ~420 nm, and the second highlighting the presence of the small peak in the Nanoparticle BpE curve at ~670 nm.

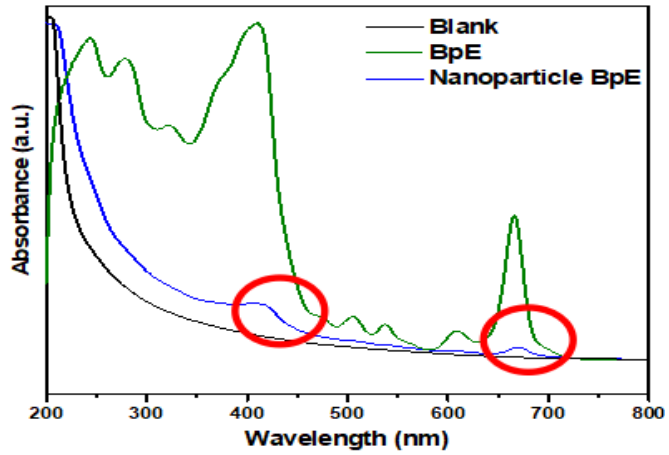


Figure **5**. UV-Vis Characterization of BpE-Loaded Polymeric Nanoparticles. UV-Vis absorption spectra of pure BpE extract (green line), blank HA-CS nanoparticles (black line), and BpE-loaded HA-CS nanoparticles (blue line). The retention of characteristic peaks at ~420 nm and ~670 nm confirms successful encapsulation.

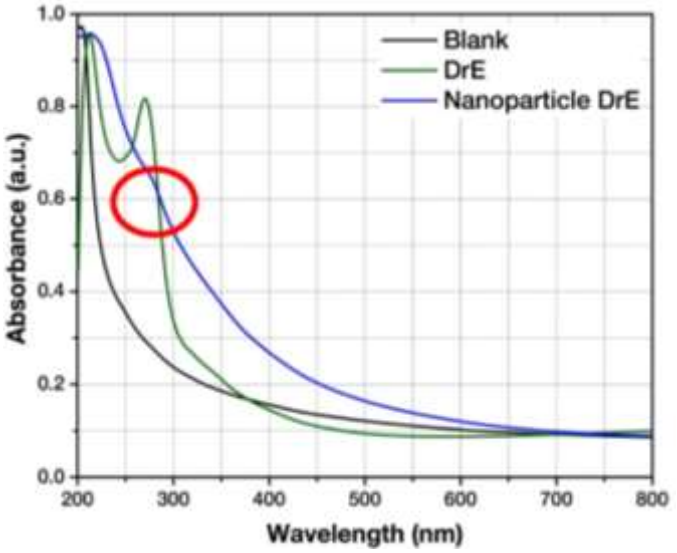


Figure **6**. UV-Vis Characterization of DrE-Loaded Polymeric Nanoparticles. UV-Vis absorption spectra of pure DrE extract (green line), blank HA-CS nanoparticles (black line), and DrE-loaded HA-CS nanoparticles (blue line).

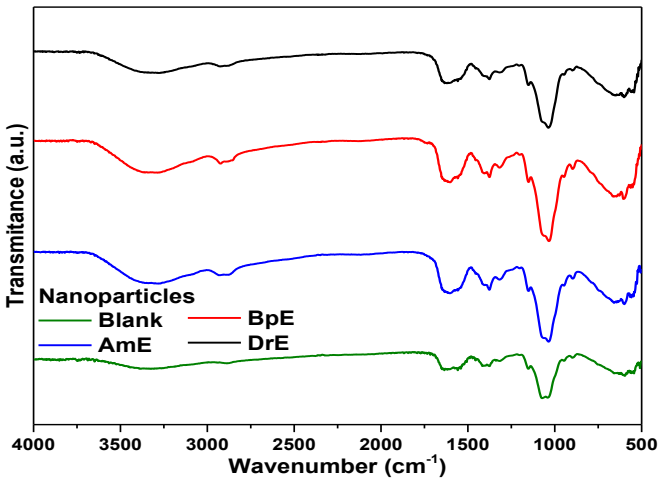


Figure **7.** FTIR spectra of blank HA-CS nanoparticles (green line), AmE-loaded PNPs (blue line), BpE-loaded PNPs (red line), and DrE-loaded PNPs.(black line) Characteristic peaks at 3300 cm^{-1} (O-H stretching), 2900 cm^{-1} (C-H stretching), 1700 cm^{-1} (C=O stretching), and 1200–1000 cm^{-1} (C-O stretching) are labeled.

3.4. Morphological evaluation of formulated nanoparticles

The morphology and structural integrity of blank nanoparticles [I] were evaluated using Scanning Electron Microscopy (SEM) and Transmission Electron Microscopy [II] (TEM) for AmE. SEM imaging revealed distinct spherical nanoparticles across all loaded formulations (AmE, BpE, and DrE). TEM [III and IV] analysis of BpE and DrE, respectively, provided high-resolution visual confirmation of a vesicle-like structure, with single particles exhibiting a well-defined boundary, suggesting a core-shell or matrix-type encapsulation. The optimization of SEM sample preparation demonstrated that applying samples directly to the grid or pin saved significant processing time without compromising image quality.

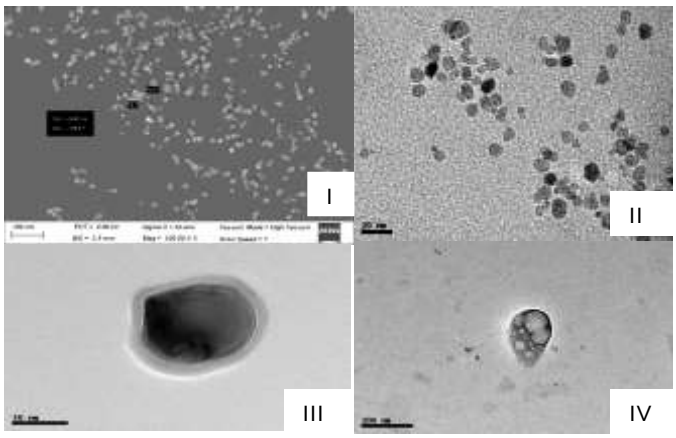


Figure **8**. Electron micrographs of HA–CS nanoparticles: (I) blank nanoparticles examined by SEM, scale bar = 100 nm; (II) TEM of AmE-loaded nanoparticles, scale bar = 20 nm; (III) TEM of BpE-loaded nanoparticle showing a defined boundary and internal contrast, scale bar = 50 nm; and (IV) TEM of DrE-loaded nanoparticle, scale bar = 100 nm.

4.0 DISCUSSION

The selection of a Hyaluronic Acid-Chitosan (HA-CS) polyelectrolyte complex (PNP) is justified by the amphiphilic nature of the matrix, which provides a hydrophobic environment for lipid-rich secondary metabolites while maintaining a hydrophilic exterior for colloidal stability (Ahmad et al., 2012). While utilizing crude extracts capitalizes on multi-target phytochemical synergy, where compounds like fatty acids, acetogenins, and steroidal saponins work in tandem, we acknowledge that whole plant matrices possess inherent compositional variability. To mitigate this in future applications, standardization via high-performance liquid chromatography (HPLC) fingerprints or chemical profiling of key index compounds will be vital to ensure reproducible encapsulation efficiencies and predictable release behaviors across distinct preparation batches.

4.1. Physicochemical stability and colloidal behaviour

Dynamic Light Scattering (DLS) confirmed the formation of nanostructures with mean diameters ranging from 344.8 nm (DrE) to 535.6 nm (AmE and BpE). The Polydispersity Index (PDI) values (0.254, 0.264, and 0.292) indicate a moderately monodisperse system (Ma et al., 2024), which is critical for ensuring predictable pharmacokinetic profiles (Anjum et al., 2023). The transition from clear polymer solutions to opalescent suspensions is a classic indicator of the electrostatic assembly between the polyanionic HA and polycationic CS. FTIR spectra further validated this assembly, showing characteristic O–H (3300 cm^{-1}) and C=O (1700 cm^{-1}) stretching, alongside the 1200–1000 cm^{-1} fingerprint region that confirms the successful integration of plant-derived alcohols and carboxylic acids within the polymeric matrix.

4.2. Confirmation of loading via UV-Vis spectroscopy

The UV-Vis characterisation (Figures 4 to 6) serves as an analytical fingerprint for extract encapsulation, best combined with encapsulation efficiency. In the BpE formulation, the retention of the ~665 nm peak, characteristic of chlorophyll-type derivatives or specific bufadienolides, within the nanoparticle spectrum (blue line) confirms that the bioactive constituents remain chemically intact after processing (Marslin et al., 2024). Similarly, the alignment of the DrE shoulder at ~270 nm with the raw extract peak provides robust evidence of successful loading. The slight spectral shifts observed are likely due to the altered electronic environment of the chromophores when confined within the HA–CS matrix, a

phenomenon typical of successful drug–polymer interactions (Mathur and Bahadur, 2024). The comparison of all FTIR spectra (Figure 7) shows that the blank HA–CS nanoparticles were dominated by the characteristic functional groups of the two polysaccharide polymers. The broad band within approximately 3200–3500 cm^{-1} was assigned to overlapping O–H stretching from hyaluronic acid and chitosan and N–H stretching from chitosan. The bands around 2850–2950 cm^{-1} were attributed to aliphatic C–H stretching. Absorptions in the 1550–1650 cm^{-1} region were associated with chitosan amide vibrations and the asymmetric stretching of the carboxylate groups of hyaluronic acid. The band around 1400 cm^{-1} was consistent with symmetric carboxylate stretching, while the 1000–1150 cm^{-1} fingerprint region represented C–O and C–O–C stretching of the HA–CS polysaccharide backbone. Compared with the blank PNP spectrum in Figure 7, the AmE-, BpE-, and DrE-loaded PNP spectra exhibited changes in band intensity, breadth, and position, particularly within the O–H/N–H, carbonyl, and polysaccharide fingerprint regions. The broadening and apparent displacement of the 3200–3500 cm^{-1} band may indicate additional hydrogen bonding between hydroxyl-containing extract constituents and the HA–CS matrix. Changes around 1650–1750 cm^{-1} may reflect contributions from carbonyl-containing phytochemicals, including acetogenins, fatty acids, esters, and related secondary metabolites. Differences in the 1000–1200 cm^{-1} region may also represent contributions from plant-derived alcohols, glycosides and saponins, although these bands overlap substantially with those of HA and chitosan.

4.3 Comparative analysis of size and stability

The polymeric nanoparticles (PNPs) developed in this study, with sizes ranging from 344.8 nm to 535.6 nm , fall within a functional range for targeted drug delivery. While these dimensions are characteristic of polysaccharide-based carriers, they are influenced by the choice of natural extracts and polymers.

4.4 Size profile and extract complexity

Similar Hyaluronic Acid-Chitosan (HA-CS) systems delivering purified compounds, such as curcuminoids, have reported smaller sizes in the range of 200–300 nm (Lin et al., 2015). The larger sizes observed for *Annona muricata* (AmE) and *Bryophyllum pinnatum* (BpE) are likely due to the complexity of using whole plant extracts (Mondal et al., 2023). These extracts contain a diverse array of phytochemicals rather than isolated molecules, which can lead to larger hydrodynamic diameters during encapsulation.

4.5 Colloidal stability

The Polydispersity Index (PDI) values of 0.254–0.292 recorded for these formulations indicate a "moderately monodisperse" system. This is consistent with other plant-based PNPs, where a PDI below 0.3 is considered a benchmark for stability and resistance to rapid aggregation in biological fluids (Anjum et al., 2023). Future studies will include the Zeta potential not included in this preliminary study. The *Dioscorea rotundata* DrE formulation achieved the smallest hydrodynamic diameter of 344.8 nm and the highest uniformity (PDI 0.254) among the three extracts. This efficiency is driven by its unique chemical profile and molecular interactions:

4.6 Natural Surfactant Properties

GC-MS analysis revealed significant concentrations of steroidal saponins and γ-sitosterol in DrE. Saponins possess amphiphilic properties that allow them to act as natural co-surfactants. By reducing interfacial tension during the complexation process, they facilitate the formation of smaller, more compact particles.

4.6.1 Efficient Molecular Packing

The steroidal structures in DrE may allow for more efficient molecular packing within the HA-CS matrix. This contrasts with the bulkier acetogenins in *Annona muricata* or the high concentration of long-chain fatty acids (over 51% combined) found in *Bryophyllum pinnatum*.

4.6.2 Electrostatic Optimization:

FTIR results for DrE identified specific alcohol and carboxylic acid functional groups. These likely provide an optimal charge density that balances the HA-CS interaction more efficiently (Lin et al., 2015). This balance prevents the over-growth of the polymer shell during the formulation process, resulting in smaller, more uniform vesicles.

4.7 **Morphological Integrity**

Morphological evaluation via SEM and TEM provided visual corroboration of the DLS data. The observation of spherical, vesicle-like structures suggests that the PNPs form a matrix-type encapsulation system. The well-defined boundaries seen in TEM images indicate that the HA-CS shell provides a robust physical barrier, which is essential for protecting volatile phytochemicals like methyl palmitate from premature degradation (Singh et al., 2024). The efficiency of the "direct-to-grid" SEM preparation method highlights a streamlined protocol for high-throughput nanoparticle characterization without sacrificing resolution.

Limitations

While this study successfully establishes the structural and spectroscopic foundation for HA-CS polysaccharide encapsulation of complex plant extracts, several limitations remain to be resolved. First, the hydrodynamic diameters (344–535 nm), though stable and reproducible, represent the upper limit for EPR-driven passive targeting. Second, while colloidal stability was verified via PDI tracking over various dilution stages, direct surface charge mapping via Zeta Potential analysis was not included in this phase of characterization. Lastly, functional biological validation, specifically *in vitro* drug release kinetics profiling, receptor-mediated cellular uptake tracking and comparative cell line cytotoxicity assays, is required to definitively prove therapeutic superiority over raw un-encapsulated extracts. These milestones are currently being pursued in our ongoing secondary research phase.

Conclusions

These results validate the use of HA-CS nanoparticles as a high-performance delivery platform for crude plant extracts. This work bridges the gap between traditional herbal medicine and modern drug delivery, offering a scalable and eco-friendly strategy to enhance the therapeutic efficacy of natural products. Future studies will focus on the in vitro release kinetics and the specific pharmacological activities of these loaded formulations against target cell lines. Future research would cover *in vitro* drug release kinetics profiles under varying physiological pH levels to simulate normal body fluid versus the acidic tumor microenvironment. Targeted cytotoxicity profiling against cancer cell lines (such as MCF-7 or MDA-MB-231 human breast cancer lines) to benchmark eukaryotic cell viability and apoptotic induction efficacy against the raw, unencapsulated extracts. Long-term colloidal stability tracking under various storage temperatures to validate commercial potential.

Highlights

- *Polymeric nanoparticles were synthesized using Hyaluronic acid and Chitosan.*
- *Extracts from* Annona muricata*,* Bryophyllum pinnatum*, and* Dioscorea rotundata *were successfully encapsulated into nanoparticles.*
- *Nanoparticles showed optimal morphology and stability via SEM and TEM.*
- *The system offers promise for plant-based smart drug delivery.*

Acknowledgements

Authors wish to thank Mujeres por Africa Foundation for the grant to Odimegwu, Joy I. that facilitated this research. We also thank the University of Castilla-La Mancha, Ciudad Real, UCLM. Spain, for hosting the fellow.

Funding

Mujeres por Africa Foundation, Spain, and IRICA, UCLM.

Competing interests

We declare that we have no competing interests

Authors' contributions

Odimegwu J. I. and Irene S. M. Rodríguez conducted the experiments. Viviana J. G. Velázquez performed the data analysis and contributed to the experimental work. Ester V. Fernández-Pacheco conceptualized the study, supervised the research, and critically reviewed and edited the manuscript. All authors reviewed and approved the final version of the manuscript.

REFERENCES

Ahmad, N., & Sharma, S. (2012). Green synthesis of silver nanoparticles using extracts of Ananas comosus. Green and Sustainable Chemistry, 2(4), 141–147. doi: 10.4236/gsc.2012.24020

Anjum, S., Abbasi, B. H., & Shinwari, Z. K. (2016). Plant-mediated green synthesis of silver nanoparticles for biomedical applications: Challenges and opportunities. Pakistan Journal of Botany, 48(4), 1731–1760.

Dash, M., Chiellini, F., Ottenbrite, R. M., & Chiellini, E. (2011). Chitosan—A versatile semi-synthetic polymer in biomedical applications. Progress in Polymer Science, 36(8), 981–1014. doi: 10.1016/j.progpolymsci.2011.02.001

Edo, G. I., Mafe, A. N., Ali, A. B. M., Akpoghelie, P. O., Yousif, E., Isoje, E. F., Igbuku, U. A., Ismael, S. A., Essaghah, A. E. A., Ahmed, D. S., Ozsahin, D. U., Umar, H., & Alamiery, A. A. (2025). Green biosynthesis of nanoparticles using plant extracts: Mechanisms, advances, challenges, and applications. BioNanoScience, 15, Article 267. doi: 10.1007/s12668-025-01883-w

Gavamukulya Y, Abou-Elella F, Wamunyokoli F, El-Shemy HA. GC-MS Analysis of Bioactive Phytochemicals Present in Ethanolic Extracts of Leaves of *Annona muricata*: A Further Evidence for Its Medicinal Diversity (2015). Pharmacognosy Journal. 7(5):300-304. 10.5530/pj.2015.5.9

Mathur, A., & Bahadur, P. S. (2024). Utilization of green synthesis for eco-friendly nanomaterials and their advanced biomedical applications in noble metal nanoparticles. Asian Journal of Applied Science and Technology, 8(2), 211–224. https://doi.org/10.38177/AJAST.2024.8220

Ma, T., Tran, T. B., Lin, E., Hunt, S., Haveman, R., Castro, K., & Lu, J. (2024). Size-transformable nanotherapeutics for cancer therapy. Acta Pharmaceutica Sinica B. https://doi.org/10.1016/j.apsb.2024.11.012

Maeda, H. (2015). Toward a full understanding of the EPR effect in primary and metastatic tumors as well as issues related to its heterogeneity. Advanced Drug Delivery Reviews, 91, 3–6. doi:https://doi.org/10.1016/j.addr.2015.01.002

Marslin, G., Siram, K., Maqbool, Q., Selvakesavan, R. K., Kruszka, D., Kachlicki, P., & Franklin, G. (2018). Secondary metabolites in the green synthesis of metallic nanoparticles. Materials, 11(6), 940. https://doi.org/10.3390/ma11060940

Merino, S., Martín, C., Kostarelos, K., Prato, M., & Vázquez, E. (2015). Nanocomposite hydrogels: 3D polymer–nanoparticle synergies for on-demand drug delivery. ACS Nano, 9(5), 4686–4697. https://doi.org/10.1021/acsnano.5b01433

Misra, R., Acharya, S., & Sahoo, S. K. (2010). Cancer nanotechnology: Application of nanotechnology in cancer therapy. Drug Discovery Today, 15(19–20), 842–850. https://doi.org/10.1016/j.drudis.2010.08.006

Moghadamtousi, S. Z., Fadaeinasab, M., Nikzad, S., Mohan, G., Ali, H. M., & Kadir, H. A. (2015). *Annona muricata* (Annonaceae): A review of its traditional uses, isolated acetogenins and biological activities. International Journal of Molecular Sciences, 16(7), 15625–15658.https://doi.org/10.3390/ijms160715625.

Mondal, A., Nayak, A., Chakraborty, P., Banerjee, S., & Nandy, B. (2023). Natural Polymeric Nanobiocomposites for Anti-Cancer Drug Delivery Therapeutics: A Recent Update. Pharmaceutics, 15(8), 2064. https://doi.org/10.3390/pharmaceutics15082064.

Mukherjee, S., Ray, S., & Thakur, R. S. (2009). Solid lipid nanoparticles: A modern formulation approach in drug delivery systems. Indian Journal of Pharmaceutical Sciences, 71(4), 349–358. doi:10.4103/0250-474X.57282.

Nwogha, J. S., Wosene, A. G., Raveendran, M., Obidiegwu, J. E., Oselebe, H. O., Kambale, R., Chilaka, C. A., & Rajagopalan, V. R. (2023). Comparative metabolomics profiling reveals key metabolites and associated pathways regulating tuber dormancy in white yam (*Dioscorea rotundata* Poir.). Metabolites, 13(5), 610. https://doi.org/10.3390/metabo13050610

Odimegwu, J. I., Olukemi, O., Alejandro, E., & Maria, E. S. (2022). Human breast tumour cells viability effect of African *Dioscorea rotundata* tuber extracts in MCF-7 and MDA-MB231 cell lines. Rep cancer Treat| Volume 6| Issue 2| doi:10.4172/Rep cancer Treat.6.2.001

Ojewole, J. A. O. (2005). Antinociceptive, anti-inflammatory and antidiabetic effects of *Bryophyllum pinnatum* (Crassulaceae) leaf aqueous extract. Journal of Ethnopharmacology, 99(1), 13–19. Doi: 10.1016/j.jep.2005.01.025

Okafor, C. E., Ijoma, I. K., Igboamalu, C. A., Ezebalu, C. E., Eze, C. F., Osita-Chikeze, J. C., Uzor, C. E. & Ekwuekwe, A. L. (2024). Secondary metabolites, spectra characterization, and antioxidant correlation analysis of the polar and nonpolar extracts of *Bryophyllum pinnatum* (Lam) Oken. BioTechnologia, 105(2), 121–136. https://doi.org/10.5114/bta.2024.139752

Onuigbo, E. B., Anozie-Ikeanyi, C., Edeh, N. E., Eze , C. O., & Gugu, T. H. (2020). Chitosan-based nanoparticles sustenance and potentiation of the antibacterial effect of ampicillin against drug resistance among strains of Escherichia coli. Journal of Biological Research and Biotechnology, 18(2), 1147-1153. https://doi.org/10.4314/br.v18i2.3

Rinaudo, M. (2006). Chitin and chitosan: Properties and applications. Progress in Polymer Science, 31(7), 603–632.https://doi.org/10.1016/j.progpolymsci.2006.06.001

Siegel, R. L., Miller, K. D., Wagle, N. S., & Jemal, A. (2023). Cancer statistics, 2023. CA: A Cancer Journal for Clinicians, 73(1), 17–48. doi: 10.3322/caac.21763

Singh, J., Dutta, T., Kim, K.-H., Rawat, M., Samddar, P., & Kumar, P. (2018). 'Green' synthesis of metals and their oxide nanoparticles: Applications for environmental remediation. Journal of Nanobiotechnology, 16, 84. doi: 10.1186/s12951-018-0408-4

Ubhenin, A. (2026). Therapeutic Symphony: *Annona muricata* Extract Orchestrates Metabolic Resilience in Mammary Carcinogenesis. Journal of Biological Research and Biotechnology, 23(2). https://doi.org/10.4314/br.v23i2.1

Wagner, H. (2011). Synergy research: Approaching a new generation of phytopharmaceuticals. Fitoterapia, 82(1), 34–37. Doi:10.1016/j.fitote.2010.11.016

World Health Organization (2024). Global cancer burden growing, amidst mounting need for services. [online] Available at: https://www.who.int/news/item/01-02-2024-global-cancer-burden-growing--amidst-mounting-need-for-services. https://www.who.int/news/item/01-02-2024-global-cancer-burden-growing--amidst-mounting-need-for-services

Yu, X., Peng, W., Wang, Y., Xu, W., Chen, W., Huang, L., Xu, H., He, X., Wang, S., Sun, Q., Lu, W., & Xu, Y. (2023). Palmitic acid inhibits the growth and metastasis of gastric cancer by blocking the STAT3 signaling pathway. Cancers, 15(2), 388. doi: 10.3390/cancers15020388.

Lin, Y., Shiya, G., Sajid, A., Guihua, L., Jue, S., Xuan, W., Qineng, P., Can, Z., & Yanyu, X. (2015). Hyaluronic acid/chitosan nanoparticles for delivery of curcuminoid and its *in vitro* evaluation in glioma cells. International Journal of Biological Macromolecules, 72, 1391–1401. https://doi.org/10.1016/j.ijbiomac.2014.10.039.

Table **1.** GC–MS profile of the ethanolic leaf extract of *Annona muricata*

Peak no.	Retention time (min)	Tentatively identified compound	Molecular formula	Relative peak area (%)
1	3.034	Unidentified	—	16.80
2	3.342	Pentadecan-2-ol (2-pentadecanol)	C15H32O	3.93
3	16.732	Oleyl alcohol	C18H36O	6.15
4	16.792	Unidentified	—	1.04
5	17.015	Butyl octyl benzene-1,2-dicarboxylate	C20H30O4	2.67
6	17.190	3,7,11,15-Tetramethylhexadec-2-en-1-ol	C20H40O	1.37
7	17.998	Hexadecanoic acid	C16H32O2	7.12
8	18.331	Ethyl hexadecanoate	C18H36O2	1.29
9	18.431	Unidentified	—	0.73
10	19.531	Phytol	C20H40O	5.61
11	19.678	(11E,13Z)-Octadeca-1,11,13-triene†	C18H32	2.15
12	19.733	(Z)-Tetradec-7-enal	C14H26O	9.39
13	19.946	Ethyl (9Z,12Z)-octadeca-9,12-dienoate	C20H36O2	3.21
14	20.003	(7Z,10Z,13Z)-Hexadeca-7,10,13-trienal	C16H26O	4.26
15	23.143	Unidentified	—	23.51
16	23.225	Unidentified	—	1.08
17	23.695	Unidentified	—	1.74
18	24.025	Diisooctyl benzene-1,2-dicarboxylate	C24H38O4	0.75
19	24.750	Unidentified	—	1.25
20	26.402	Unidentified	—	1.54
21	28.350	Unidentified	—	1.12
22	28.567	Unidentified	—	0.74
23	28.875	Unidentified	—	0.85
24	29.331	Unidentified	—	0.74
25	29.704	Unidentified	—	0.95
		Total		**100.00**

Gavamukulya et al., 2015.

Table **2.** GC–MS profile of *Bryophyllum pinnatum* plant extracts (polar)

Retention time (min)	Peak area (%)	Tentatively identified compound	Library/ID reference no.	CAS no.	Spectral match quality (%)
11.0425	0.2117	Oxalic acid, dodecyl 3,5-difluorophenyl ester	220479	1000309-67-7	55
11.3875	0.1726	Cyclotetradecane	61849	000295-17-0	80
11.4276	0.1038	Heptafluorobutyric acid, pentadecyl ester	248207	959261-23-5	46
11.7394	0.7246	4-Tetradecyne	59854	060212-33-1	66
12.1181	0.9465	9-Eicosenoic acid, (Z)-	169286	029204-02-2	60
12.3156	1.1888	Cetene	87833	000629-73-2	91
12.4157	0.2007	5-Tetradecene, (Z)-	61856	041446-62-2	89
12.7666	2.2159	7,11-Hexadecadienal	98680	1000130-85-7	70
12.8261	0.5946	cis-11-Hexadecenal	100562	053939-28-9	89
13.1249	7.2367	9-Octadecene, (E)-	113637	007206-25-9	95
13.3440	4.3526	Hexadecane	89838	000544-76-3	96
15.7278	0.3700	2,6,10,14-Tetramethylpentadecane	128856	001921-70-6	98
16.9475	0.3744	Cyclohexadecane	87836	000295-65-8	93
17.0796	0.5372	2-Octyl-1-dodecanol	158035	005333-42-6	60
17.5264	8.2354	1-Octadecene	113634	000112-88-9	99
17.9181	15.6447	Tritetracontane	273205	007098-21-7	94
18.7907	0.4289	2-Cyclohexylundecane	100622	013151-77-4	55
18.9506	0.8331	9-Heptadecanone	115513	000540-08-9	99
20.0611	1.7729	Methyl hexadecanoate	130813	000112-39-0	98
20.2932	0.3271	Dibutyl phthalate	138056	000084-74-2	64
20.4569	0.5115	Heptadecyl heptafluorobutyrate	256997	959085-66-6	78
20.6400	0.7674	Heptadecyl pentadecafluorooctanoate	274382	1000406-04-7	78
20.8738	1.0267	Cyclopentadecane	74572	000295-48-7	91
21.7143	7.5731	9-Eicosene, (E)-	140276	074685-29-3	93
23.1252	0.2334	Methyl 9,12-octadecadienoate	153873	002462-85-3	99
23.2984	1.1222	Methyl 11-octadecenoate	155737	052380-33-3	99
23.8914	0.1226	Methyl stearate	157884	000112-61-8	95
26.4361	0.1211	1,19-Eicosadiene	138504	014811-95-1	58
26.5750	0.1416	Fumaric acid, cis-hex-3-enyl hexadecyl ester	247784	1000348-87-1	46
28.6495	0.1449	Cyclotetracosane	194001	000297-03-0	99
29.8794	6.6881	1-Docosene	167463	001599-67-3	99
29.9774	0.1346	1,1′:4′,1″-Tercyclohexane	109947	001795-19-3	64
30.5382	4.4943	Diisooctyl phthalate	233366	000131-20-4	91
30.7995	16.3975	3-Eicosene, (E)-	140277	074685-33-9	99
30.9419	1.4327	Erucic acid	195585	000112-86-7	93
31.1150	3.4922	Oleic acid	142069	000112-80-1	91
31.3752	1.4305	9-Tricosene, (Z)-	180806	027519-02-4	90
31.6721	3.2286	Glyceryl monooleate [9-octadecenoic acid (Z)-, 2,3-dihydroxypropyl ester]	210562	000111-03-5	89
31.7797	4.4650	5-Eicosene, (E)-	140275	074685-30-6	95

Okafor et al., 2024.

Table **3.** GC–MS profile of *Bryophyllum pinnatum* plant extracts (nonpolar)

Retention time (min)	Peak area (%)	Tentatively identified compound	Library/ID reference no.	CAS no.	Spectral match quality (%)
17.5090	0.3031	17-Pentatriacontene	265113	006971-40-0	87
17.6971	0.1618	Carbonic acid, octadecyl prop-1-en-2-yl ester	209053	1000383-11-5	58
18.9768	0.3316	Eicosyl octyl ether	243191	1000406-38-8	49
19.4046	0.6115	Methyl 2-octynoate	28541	000111-12-6	38
19.7076	0.1106	Cyclotridecane	49687	000295-02-3	74
20.0652	4.2923	Methyl 14-methylpentadecanoate	130843	005129-60-2	97
21.5259	0.6029	Trichloroacetic acid, pentadecyl ester	221903	074339-53-0	93
21.6713	0.3578	7-Hexadecenal, (Z)-	100566	056797-40-1	62
22.2116	1.8153	9-Octadecenoic acid, (E)-	142088	000112-79-8	72
22.8113	3.0989	10-Bromoundecanoic acid	124097	018294-93-4	58
23.1140	8.9796	Methyl 9,12-octadecadienoate	153873	002462-85-3	99
23.2719	19.2819	Methyl 11-octadecenoate	155737	052380-33-3	99
23.8768	4.1406	Methyl 15-methylheptadecanoate	157952	054833-55-5	95
25.2397	17.2066	Z,Z-6,13-Octadecadien-1-ol acetate	167383	1000131-07-0	80
26.0010	10.2243	Oleic acid	142070	000112-80-1	95
26.2701	8.2674	7,11-Hexadecadienal	98680	1000130-85-7	87
26.6171	10.2561	12-Methyl-E,E-2,13-octadecadien-1-ol	140258	1000130-90-4	56
27.0864	4.2380	cis-13-Octadecenoic acid	142083	013126-39-1	60
27.3800	3.3145	9-Tetradecenal, (Z)-	74488	053939-27-8	93
30.4934	0.9576	Diisooctyl phthalate	233366	000131-20-4	58
34.8112	0.4519	1,5,9-Undecatriene, 2,6,10-trimethyl-, (Z)-	57864	062951-96-6	74
38.3657	0.9957	3,6-Dimethyl-5-oxo-1,2,3,5-tetrahydroimidazo[1,2-a]pyrimidine	35878	058910-42-2	70

Okafor et al., 2024.

Table 4 GC–MS Metabolite Mapping in *Dioscorea rotundata*

GC–MS library query	Chemical functional group	HMDB ID	PubChem CID	KEGG ID
9,12,15-Octadecatrienoic acid, (Z,Z,Z)-	Fatty acids	HMDB0001388	5280934	C06427
Ethylenediamine-N,N′-dipropionic acid	Flavonoids	HMDB0015109	6049	C00284
1-Butanol, 2-methyl-, acetate	Esters	HMDB0032385	6658	C19504
Tetraacetyl-d-xylonic nitrile	Amino Acids and Derivatives	HMDB0000271	1088	C00213
(+)-N-Acetylmuramic acid	nucleotide-sugar	HMDB0011720	24755495	C01050
1-Butanol, 3-methyl-, formate	Fatty esters	HMDB0034163	8052	C12293
1,3-Propanediol, 2-ethyl-2-(hydroxymethyl)-	Alcohols and Polyols	HMDB0031320	7896	C20335
1,8-Di(4-nitrophenylmethyl)-3,6-diazahomoadamantan-9-one	Amino Acids and Derivatives	HMDB0000306	5610	C00483
Benzeneethanamine, 2-fluoro-á,3,4-trihydroxy-N-isopropyl-	Amines, Aromatic	HMDB0012275	1001	C05332
Desulphosinigrin	Flavonoids		47205615	C16307
Glycerin	Alcohols and Polyols	HMDB0000131	753	C00116
9,12-Octadecadienoic acid (Z,Z)-	Lipids	HMDB0000673	5280450	C01595
Dasycarpidan-1-methanol, acetate (ester)	Flavonoids	HMDB0001859	1983	C06804
2,2,4-Trimethyl-1,3-pentanediol diisobutyrate	Alcohols	HMDB0034472	7662	C02008
Sucrose	Disaccharides	HMDB0000258	5988	C00089
5-O-Methyl-d-gluconic acid dimethylamide	Phytohormone	HMDB0002390	6738	C14088
2,6-Dioxa-tricyclo [3.3.2.0(3,7)] decan-9-one	Amines	HMDB0001925	3672	C01588
1,3-Cyclohexanedione, 2,5,5-trimethyl-	Alcohols		10263	C08063
5-Methoxypyrrolidin-2-one	Alkaloids	HMDB0006790	656504	C05401
2(3H)-Furanone, 5-heptyldihydro	Sugar Acids	HMDB0002541	5640	C03383
2-Propanol, 1,1′-oxybis-	Amino Alcohols	HMDB0001849	4946	C07407
10-Hydroxydecanoic acid	Fatty Acids	HMDB0002059	79034	C08317
Succinamide	Biogenic Polyamines	HMDB0001414	1045	C00134
2-Octenoic acid, 4,5,7-trhydroxy	Carboxylic Acids	HMDB0033977	7294	C19443
2-Hydroxy-3-methoxy-succinic acid, dimethyl ester	carboxylic acid	HMDB0000156	222656	C00149
Octanoic acid, 2-phenylethyl ester	Benzene Derivatives	HMDB0034240	7501	C19506
2-Cyclohexen-1-one, 4-(3-hydroxy-1-butenyl)-3,5,5-trimethyl-	Terpenoids	HMDB0030500	2171	C06827
8-Hydroxy-7-methoxycoumarin	Coumarins	HMDB0015497	4632	C14285
Pyrimidine-4,6-diol, 5-methyl-	Nucleic Acids and Derivatives	HMDB0000300	1174	C00106
Oxime-, methoxy-phenyl-_	phenols	HMDB0003791	119219	C04043
Adenine	Nucleotides	HMDB0000034	190	C00147
2,5-Cyclohexadiene-1,4-dione, dioxime	Benzoquinones	HMDB0003364	4650	C00472
2,5-Pyrrolidinedione, 3-(1-aminoethylidene)-4-methyl-	Alkaloids	HMDB0004290	440899	C06051
Phthalic acid, hept-4-yl isobutyl ester	Carboxylic Acids	HMDB0015175	92142	C07910
L-Glutamine	Amino Acids and Derivatives	HMDB0000641	5961	C00064
Methyl cis-13,16-Docosadienate	carboxylic acid	METPA0268		C02295
2-Hydroxyhippuric acid-3TMS	Phytohormone	HMDB0000840	10253	C07588
2,4-Di-tert-butylphenoxytrimethylsilane	Amines	HMDB0015223	2484	C08067
Pentasiloxane, dodecamethyl-	organosiloxane	HMDB0062731	8853	

Nwogha et al., 2023.